Published in final edited form as:

Cancer Res. 2018 January 01; 78(1): 36–50. doi:10.1158/0008-5472.CAN-17-1352.

Adaptive evolution of the GDH2 allosteric domain promotes gliomagenesis by resolving IDH1^{R132H} induced metabolic liabilities

Matthew S. Waitkus[1,2], **Christopher J. Pirozzi**[1,2], **Casey J. Moure**[1,2], **Bill H. Diplas**[1,2], **Landon Hansen**[1,2], **Austin Carpenter**[1,2], **Rui Yang**[1,2], **Zhaohui Wang**[1,2], **Brian O. Ingram**[3], **Edward D. Karoly**[3], **Robert P. Mohney**[3], **Ivan Spasojevic**[4,5], **Roger E. McLendon**[1,2], **Henry S. Friedman**[2,6], **Yiping He**[1,2], **Darell D. Bigner**[2,6], and **Hai Yan**[1,2,7]

[1]Department of Pathology, Duke University, Durham, NC

[2]Preston Robert Tisch Brain Tumor Center, Duke University Medical Center, Durham, NC

[3]Metabolon Inc., Research Triangle Park, NC

[4]Department of Medicine – Oncology, Duke University School of Medicine

[5]Pharmacokinetics/Pharmacodynamics Core Laboratory, Duke Cancer Institute

[6]Department of Neurosurgery, Duke University Medical Center, Durham, NC

Abstract

Hot-spot mutations in the isocitrate dehydrogenase 1 (*IDH1*) gene occur in a number of human cancers and confer a neomorphic enzyme activity that catalyzes the conversion of α-ketoglutarate (αKG) to the oncometabolite D-(2)-hydroxyglutarate (D2HG). In malignant gliomas, IDH1^{R132H} expression induces widespread metabolic reprogramming, possibly requiring compensatory mechanisms to sustain the normal biosynthetic requirements of actively proliferating tumor cells. We used genetically engineered mouse models of glioma and quantitative metabolomics to investigate IDH1^{R132H}-dependent metabolic reprogramming and its potential to induce biosynthetic liabilities that can be exploited for glioma therapy. In gliomagenic neural progenitor cells, IDH1^{R132H} expression increased the abundance of dipeptide metabolites, depleted key tricarboxylic acid (TCA) cycle metabolites, and slowed progression of murine gliomas. Notably, expression of glutamate dehydrogenase GDH2, a hominoid-specific enzyme with relatively restricted expression to the brain, was critically involved in compensating for IDH1^{R132H}-induced metabolic alterations and promoting IDH1^{R132H} glioma growth. Indeed, we found that recently evolved amino acid substitutions in the GDH2 allosteric domain conferred its non-redundant, glioma-promoting properties in the presence of IDH1 mutation. Our results indicate that among the unique roles for GDH2 in the human forebrain is its ability to limit IDH1^{R132H}-mediated metabolic liabilities, thus promoting glioma growth in this context. Results from this study raise the possibility that GDH2-specific inhibition may be a viable therapeutic strategy for gliomas with *IDH* mutations.

[7]Address correspondence to: Hai Yan, M.D., Ph.D., Phone: (919) 668-7850; hai.yan@duke.edu, Duke University Medical Center, 199B-MSRB Building, Research Drive, Durham, North Carolina 27710.

INTRODUCTION

Missense mutations in isocitrate dehydrogenase 1 and 2 (IDH1/2) occur in a number of human cancers, including acute myeloid leukemia (1), intrahepatic cholangiocarcinoma (2), chondrosarcoma (3), and malignant glioma (4–6). The vast majority of secondary glioblastomas and diffuse grade II–III gliomas harbor heterozygous missense mutations in *IDH1* and *IDH2*, with $IDH1^{R132H}$ as the most common change (5). Whereas $IDH1/2^{WT}$ catalyzes the oxidative decarboxylation of isocitrate to α-ketoglutarate (αKG), mutations in the active site of these enzymes, codon 132 of IDH1 or codons 140 or 172 of IDH2, confer a neomorphic enzyme activity that catalyzes the conversion of αKG to the oncometabolite D-(2)-hydroxyglutarate (D2HG) (7). D2HG is an inhibitor of αKG-dependent dioxygenases and is thought to promote malignancy by altering epigenetics, blocking differentiation, and creating a cellular state permissive to malignant transformation (8–12).

In addition to producing D2HG, $IDH1^{R132H}$ alters the metabolic flux of isocitrate and αKG and induces widespread metabolic reprogramming, including alterations in glutaminolysis and reductive glutamine metabolism under hypoxia (13–16). As a consequence of $IDH1^{R132H}$-dependent D2HG production, glioma cells may undergo compensatory metabolic changes to sustain biosynthetic requirements during proliferation (14–16). For example, $IDH1^{R132H}$-expressing glioma cells exhibit increased glutaminolysis (16), a mechanism that replenishes αKG levels and increases reductive glutamine metabolism for lipid synthesis (15). Furthermore, inhibitors of glutaminase, the enzyme that catalyzes the first step in the conversion of l-glutamine → l-glutamate → αKG, inhibit the growth of glioma and leukemia cells that harbor *IDH1/2* mutations (17,18), suggesting that glutaminolysis may be therapeutically targetable in glioma patients. Indeed, intensive efforts are underway to develop drug candidates that target enzymes involved in cancer cell metabolism, including inhibitors of both wild-type and mutant IDH1/2 (19,20). However, the therapeutic potential of exploiting the metabolic liabilities present in *IDH1*-mutated tumors remains incompletely understood. To advance our understanding of this approach, it is important that clinically relevant animal models are used to further inform the selection of therapeutic targets, as well as the rational design and development of novel pharmacological agents for targeting cancer cell metabolism. In the context of IDH1 mutations, the ratio of $IDH1^{WT}$ to $IDH1^{R132H}$ may be a critical determinant of D2HG production and metabolic reprogramming (21), and it is therefore critical that genetically faithful heterozygous $IDH1^{R132H/WT}$ models are employed in preclinical studies.

A number of recent studies reported that *IDH1* mutations co-occur with p53 (*TP53*) loss-of-function mutations in the vast majority of adult grade II/III astrocytomas (22–25). In this study, we generated a genetically faithful mouse model of human astrocytoma using engineered neural progenitor cells (NPCs) harboring a heterozygous $IDH1^{R132H/WT}$ mutation in the context of *TP53* deletion, and we used this model to study $IDH1^{R132H}$-dependent metabolic reprogramming and its potential to elicit metabolic liabilities that can be exploited for glioma therapy. We found that $IDH1^{R132H}$ expression in gliomagenic NPCs (GPCs) increases the abundance of numerous dipeptide metabolites, depletes several key tricarboxylic acid (TCA) cycle metabolites, and slows growth of murine gliomas in vivo. By examining RNA-seq data from The Cancer Genome Atlas (TCGA) of enzymes involved in

glutaminolysis, we identified glutamate dehydrogenase 2 (GDH2) as a critical enzyme involved in compensating for $IDH1^{R132H}$-induced metabolic liabilities and promoting $IDH1^{R132H}$ glioma growth. Importantly, we found that the ability of GDH2 to promote growth of $IDH1^{R132H}$-expressing gliomas is not shared by the housekeeping enzyme glutamate dehydrogenase 1 (GDH1). Using site-directed mutagenesis coupled with cell growth and intracranial tumor models, we identified two amino acids in the GDH2 allosteric domain that confer this non-redundant, glioma-promoting function in vitro and in vivo. These studies provide evidence that the evolutionary adaptations of GDH2 that optimize glutamate turnover in the hominoid forebrain (26–28) may also drive the growth of IDH-mutant brain tumors, and may help to guide the design of GDH2-specific inhibitors for glioma therapy.

MATERIALS AND METHODS

Genetically Engineered Mice and NSC Lines

$IDH1^{R132H}$ conditional knock-in mice were generated as previously described (29). A targeting vector based off of the genomic sequence of the 129P2/Ola mouse strain was generated containing the following features: a 5,426-base pair 5′ homology arm encompassing exon 2 of *IDH1* followed by a LoxP site, three copies of the SV40 polyadenylation signal, a neomycin resistance gene flanked with FRT sites, another LoxP site, and a 2,416-base pair 3′ homology arm encompassing exon 3 of *IDH1* and the R132H mutation. A two-base pair change from the CGA codon for arginine to the CAC codon for histidine was produced. This construct was electroporated into 129P2/Ola mouse embryonic stem cells and recombinants were selected using G418. PCR across the 3′ homology arm was performed to distinguish homologous recombinants from non-homologous integrants. $TP53^{fl/fl}$ animals were generously provided by Dr. Rob Wechsler-Reya and were crossed into the IDH1-R132H conditional knock-in mouse model. Animals were maintained in a barrier facility (Duke Cancer Center Isolation Facility) and were maintained according to NIH guidelines. The animals were kept under pathogen-free conditions in sterilized plastic containers and were monitored daily. To create NSC lines from genetically engineered mice, pregnant dams were euthanized via CO2 asphyxiation followed by extraction of E14.5 embryos. Embryos were decapitated and placed in dissection media (2% glucose on ice) and forebrains were harvested under a dissection microscope, and mechanically triturated in NeuroCult Proliferation media (Stem Cell Technologies) and spun down at 150G for 5 minutes. Cells were resuspended in NeuroCult proliferation media and filtered through a 40μM filter, after which they were plated at a density of 1×10^5 cells per cm^2. Recombination of floxed alleles was induced by Cre-recombinase, delivered 24 hours after cell isolation using a Cre-expressing RGD fiber-modified adenovirus (Vector Biolabs, 1769) or GFP-expressing adenovirus (Vector Biolabs, 1768) at 10 MOI.

Genotyping

For NSC genotyping, E14.5 tissue was lysed overnight at 55° Celsius in lysis buffer (100mM Tris-HCl pH 8; 5mM EDTA pH 8; 0.0% SDS; 200mM NaCl; Proteinase K, and water). Solution containing tissue was vortexed and centrifuged at 14,000G for 10 minutes. Supernatant was added to an equal volume of isopropanol and gently inverted until a

precipitate formed. The precipitate was transferred to 300μl 70% Ethanol, inverted, and centrifuged at 14,000G for 10 minutes. Supernatant was removed and pellet was air dried for 10 minutes. Pellet was resuspended in 50 to 100μl of sterile H2O and further diluted 1:50 in sterile H2O. 1.5μl of diluted DNA were used for PCR reactions. PCR master mixes contained the following: 1× Kapa Buffer A, 0.2mM dNTP, 6% DMSO, 1uM of forward primer, 1uM of reverse primer, and 0.3U Kapa2G Fast polymerase from Kapa Biosystems. Touchdown PCR protocol was performed: 1× (95°C 5 minutes); 3× (95°C 20 seconds, 64°C 20 seconds, 72°C 20 seconds), 3× (95°C 20 seconds, 61°C 20 seconds, 72°C 20 seconds), 3× (95°C 20 seconds, 57°C 20 seconds, 72°C 20 seconds), 30× (95°C 20 seconds, 55°C 20 seconds, 72°C 20 seconds), 1× (72°C 5 minutes). Primer sequences: IDH1-GGCTGGCCTCACACTCAAGAGAT, GCAGATCTGCAAGCTTCTGTGGAA, GCCAGTTAGTCATAGGGTGAACCTTCC; P53-GGTTAAACCCAGCTTGACCA, GGAGGCAGAGACAGTTGGAG.

Ethics Statement

Studies involving the use of animal models were approved by the Institutional Animal Care and Use Committee of Duke University, an institution accredited by the Association for Assessment and Accreditation of Laboratory Animal Care (AAALAC), International. Protocol numbers: A072-13-03 and A037-16-02.

Animal Studies and Intracranial Transplantation Surgeries

Studies involving transplantation of murine glioma progenitor cells (GPCs) were performed using adult (6–8 week old) male NOD-SCID-γ mice. Studies involving the transplantation of patient-derived 08-0537 $IDH1^{R132H/WT}$ cells were performed using adult male outbred nude mice. All mice were purchased from the Duke University Mouse Breeding Core Facility. After surgery, animals were monitored daily for the onset of neurological symptoms, including inability to ambulate, ataxia, seizures, weight loss, prolonged inappetence, or loss of consciousness. Adult animals were euthanized (via CO2 asphyxiation or through a lethal dose of Urethane (10 μl/g of 20% Urethane in sterile PBS). Once unresponsive, animals underwent intracardiac perfusion with 15 mL PBS followed by 15 mL of 10% Neutral Buffered Formalin. Tissues were harvested and post-fixed in 10% Neutral Buffered Formalin for 24 hours and transferred to 70% Ethanol for paraffin embedding.

To prepare neural stem cells or patient-derived glioma cells for intracranial transplantation, cells were triturated and filtered through a 40 μm mesh filter to achieve a single cell suspension. Cells were spun down by low-speed centrifugation and resuspended in 3% methylcellulose in neurobasal medium. Mice were placed in a Stoelting sterotactic injection device under isoflurane-induced anesthesia. An incision was made in the midline of the scalp over the position of the frontal cortex, and bregma was located visually. Cells were injected 2mm right and 3.5 mm deep relative to Bregma using a 25-gauge needle, and the needle was raised ~.5 mm. After one minute, the syringe was slowly removed to prevent efflux. The site of injection was then sealed with bone wax, Marcaine was administered as a local anesthetic, and the incision was sealed with surgical glue.

Immunofluorescence and Imaging

For confocal immunofluorescence imaging, 08-0537 cells were seeded onto laminin-coated chamber slides and allowed to adhere overnight in Neurocult NS-A NSC proliferation media supplemented with EGF (20 ng/ml) FGF (10 ng/ml) and heparin (0.0002%) (Stem Cell Technologies). 24 hours after plating, media was aspirated off and cells were washed once with ice-cold PBS, followed by fixing with 4% formaldehyde for 15 minutes at room temperature. Cells were washed 3 times with ice-cold PBS and permeablized with ice-cold 100% methanol 10 minutes at −20°C. Slides were rinsed in PBS 3 times for 5 minutes. Slides were incubated with with blocking buffer (1× PBS, 5% goat serum, 0.3% Triton X-100) for one hour at 4°C. Primary anti-GLUD1/2 (Cell Signaling #12793) and anti-Cytochome C (Cell Signaling #12963) were diluted in antibody dilution buffer (1× PBS, 1% BSA, 0.3% Triton™ X-100) and incubated on the slides overnight at 4°C. The next day, slides were washed 3× with antibody dilution buffer. Anti-mouse IgG Alexa-Fluor-488 and anti-rabbit IgG Alexa-Fluor-568 (ThermoFisher) were diluted in antibody dilution buffer and incubated on the slides for 2 hours at 4°C. Slides were then washed 3× with ice-cold PBS, stained with DAPI in ultrapure H_2O, washed 3× with PBS and mounted with coverslips using Prolong Antifade reagent. Slides were imaged using a Zeiss 780 upright laser-scanning confocal microscope under 63× oil immersion lens. The system was purchase with funding from the NIH/NCRR Shared Instrumentation Grant 1S10-RR027867-01

Western blotting

Total cell lysate from containing ~20 μg total protein was resolved using Bis-Tris buffered SDS-PAGE gels ranging from 8–12% depending on the protein of interest. Gels were soaked in protein transfer buffer (48 mM Tris, 39 mM glycine, 20% methanol, 0.0375% SDS) and transferred to a PVDF membrane using a BioRad Mini Tran-Blot transfer cell. After transfer, PVDF membranes were washed briefly in TBST (150 mM NaCl, 50 mM Tris-HCl, pH7.5, 0.1% Tween-20) and then blocked for 2 hours in Pierce TBST Protein-Free blocking buffer (Cat # 37571). After blocking, primary antibodies were diluted 1:1000 in TBST blocking buffer and incubated overnight at 4°C. GAPDH antibodies were diluted at 1:5000. Membranes were washed and then incubated with horseradish peroxidase (HRP) conjugated secondary antibody for one hour and HRP signals were detected by chemiluminescence using the BioRad ChemiDoc MP sytem. The anti-$IDH1^{WT}$ monoclonal antibody used for western blotting was purchased from Cell Signaling Technology (Catalog #8137) and the $IDH1^{R132H}$-specific antibody was purchased from Dianova (DIA-H09).

Retrovirus Generation and Transgene Expression

Retroviral particles for transgene delivery were generated using HEK293FT cells. HEK293FT cells were split to ~80% confluency, and cells were transfected 24 hours later with pGag/Pol (12 μg), pVSV/G (5 μg), and expression vector (MIGR1 or MIGR1-PDGFB, 7 μg) using Lipofectamine 2000 in 7 ml of OPTI-MEM. 8 hours later, transfection media was replaced with full growth media. 16 hours after addition of full growth media, full growth media was replaced with NSC proliferation media (containing EGF and Stem Cell Technologies NSC proliferation supplement). 24 hours after incubating in NSC proliferation media, conditioned supernatant was collected, spun at 3000 rpm to remove debris, and used

to infect NSCs. 80,000 NSCs were seeded in a 24 well dish in 450 μl NSC growth media, and 50 μl of viral particle-containing supernatant was added to the well for 36 hours. After this incubation, NSCs were resuspended and washed to remove viral particles, and NSCs were then split into fresh NSC growth media. Murine $IDH1^{WT}$ and $IDH1^{R132H}$ and human GDH1 and GDH2 transgenes were cloned into MIGR1 retroviral expression vectors in which the transgenes were placed under control of an MSCV promoter. MIGR1 contains an internal ribosome entry site, located on the 3′ side of the transgene, followed by a GFP reporter to monitor retroviral transduction efficiency and transgene expression.

Cellular Proliferation Assays

NSC proliferation assays were performed using the CyQuant Assay kit according to the manufacturer's instructions. Briefly, 1,000 NPCs or were seeded into laminin-coated microplates and allowed to proliferate for 4 days in low-glucose NSC proliferation media. Proliferation media was aspirated off the plates and cells were frozen at −80°C overnight. Microplates were removed from the freezer and allowed to reach room temperature, after which CyQuant GR dye diluted in lysis buffer was added to the plate for 5 minutes, after which the plates were imaged using a fluorescence microplate reader. For 08-0537 proliferation assays, 5×10^3 cells were seeded into laminin-coated microplates in 100 μL media volume and allowed to adhere for 16 hours. 100 μL of fresh proliferation media containing DMSO or AGI-5198 (5 μM final concentration) was then added to culture media and cells were allowed to proliferate for 8 days, with a media change 96 hours after seeding. After 8 days of proliferation, media was aspirated off the plates and cells were frozen at −80°C for the CyQuant assay, as described above.

Metabolomic Analysis of Neural Stem Cells

Metabolomic profiling was performed in collaboration with Metabolon Inc (Research Triangle Park, NC).

Cellular Samples—NSCs were passaged as a single cell suspension into fresh NSC proliferation media and allowed to proliferate for 48 hours. Cells were spun down at 150xG for 3 minutes and conditioned media was removed and archived for future analyses. Pellets were snap frozen in a dry-ice/ethanol slurry and placed at −80°C.

Ultrahigh Performance Liquid Chromatography-Tandem Mass Spectroscopy (UPLC-MS/MS)—All methods utilized a Waters ACQUITY ultra-performance liquid chromatography (UPLC) and a Thermo Scientific Q-Exactive high resolution/accurate mass spectrometer interfaced with a heated electrospray ionization (HESI-II) source and Orbitrap mass analyzer operated at 35,000 mass resolution. The sample extract was dried then reconstituted in solvents compatible to each of four methods. Each reconstitution solvent contained a series of standards at fixed concentrations to ensure injection and chromatographic consistency. One aliquot was analyzed using acidic positive ion conditions, chromatographically optimized for more hydrophilic compounds. In this method, the extract was gradient eluted from a C18 column (Waters UPLC BEH C18-2.1×100 mm, 1.7 μm) using water and methanol, containing 0.05% perfluoropentanoic acid (PFPA) and 0.1% formic acid (FA). Another aliquot was also analyzed using acidic positive ion conditions,

however it was chromatographically optimized for more hydrophobic compounds. In this method, the extract was gradient eluted from the same afore mentioned C18 column using methanol, acetonitrile, water, 0.05% PFPA and 0.01% FA and was operated at an overall higher organic content. Another aliquot was analyzed using basic negative ion optimized conditions using a separate dedicated C18 column. The basic extracts were gradient eluted from the column using methanol and water, however with 6.5mM ammonium bicarbonate at pH 8. The fourth aliquot was analyzed via negative ionization following elution from a HILIC column (Waters UPLC BEH Amide 2.1×150 mm, 1.7 μm) using a gradient consisting of water and acetonitrile with 10mM ammonium formate, pH 10.8. The MS analysis alternated between MS and data-dependent MS^n scans using dynamic exclusion. The scan range varied slighted between methods but covered 70–1000 m/z. Raw data files are archived and extracted as described below.

Data Extraction and Compound Identification—Raw data was extracted, peak-identified and QC processed using Metabolon's hardware and software. These systems are built on a web-service platform utilizing Microsoft's .NET technologies, which run on high-performance application servers and fiber-channel storage arrays in clusters to provide active failover and load-balancing. Compounds were identified by comparison to library entries of purified standards. Metabolon maintains a library based on authenticated standards that contains the retention time/index (RI), mass to charge ratio (*m/z*), and chromatographic data (including MS/MS spectral data) on all molecules present in the library. Furthermore, biochemical identifications are based on three criteria: retention index within a narrow RI window of the proposed identification, accurate mass match to the library +/− 10 ppm, and the MS/MS forward and reverse scores between the experimental data and authentic standards. The MS/MS scores are based on a comparison of the ions present in the experimental spectrum to the ions present in the library spectrum. While there may be similarities between these molecules based on one of these factors, the use of all three data points can be utilized to distinguish and differentiate biochemicals.

Curation—A variety of curation procedures were carried out to ensure that a high quality data set was made available for statistical analysis and data interpretation. The QC and curation processes were designed to ensure accurate and consistent identification of true chemical entities, and to remove those representing system artifacts, mis-assignments, and background noise. Metabolon data analysts use proprietary visualization and interpretation software to confirm the consistency of peak identification among the various samples. Library matches for each compound were checked for each sample and corrected if necessary.

Metabolite Quantification and Data Normalization—Peaks were quantified using area-under-the-curve measurements. To account for differences in metabolite levels due to differences in the amount of material present in each sample, the biochemical data was normalized according to total protein (Bradford assay). One-way analysis of variance and Tukey's post-hoc test was used to evaluate differences between experimental groups for metabolites in each cell line experiment, and multiplicity adjusted p-values are reported as *$p<0.05$, **$p<0.01$, ***$p<0.001$. For comparisons between group averages presented in

Supplemental Datasets A and B, Welch's two-sample *t*-test was used to identify biochemicals that differed significantly between experimental groups.

Analysis of D2HG

Quantification of D2HG in biological media/tissues was done by liquid chromatography-electron spray ionization-tandem mass spectrometry (LC-ESI-MS/MS) method as published by Struys et al., with modifications to accommodate different equipment and sample matrices (30).

Materials—D2HG and Diacetyl-L-tartaric anhydride (DATAN) were purchased from Sigma/Aldrich. Racemic mixture of L- and D2HG-d4 was prepared by mixing 1 mg of α-ketoglutarate-d6 (Sigma/Isotec) with 1 mg of $NaBH_4$ (Sigma) in 0.2 mL anhydrous MeOH (Sigma) followed by 30-minute incubation at 60°C. Sodium hydroxide (25%) and formic acid (98%) were from Fluka, Germany (mass spectrometry grade). Other reagents and solvents were of analytical grade.

Sample preparation/derivatization—To 20 μL of sample, 10 μL of 20 μg/mL of each L/D-2-HG-d4 (internal standard) in water was added and the mixture was evaporated to dryness under gentle stream of nitrogen at 65°C. The dry residue was treated with 50 μL of 50 mg/mL of freshly prepared DATAN in dichloromethane/glacial acetic acid (4/1 by volume) and heated at 75°C for 30 min. After drying (65°C, 1h) the residue was dissolved in 20 μL LC mobile phase (see below) for LC/MS/MS analysis.

LC/MS/MS analysis—Instrument: Shimadzu 20A series HPLC and Sciex/Applied Biosystems API 4000 QTrap. Mobile phase (isocratic elution): water, 3% acetonitrile, 0.5% methanol, 2mM ammonium hydroxide, pH adjusted to 3.6 by formic acid. Analytical column: ACE #ACE-111-1546 (C_{18}, 150 × 4.6mm), and #ACE-111-0103GD guard column. Column temperature: 45°C. Run time: 4 min. Injection volume: 5 μL. Mass spectrometer parameters (voltages, gas flow, and temperature) were optimized by infusion of 100 ng/mL of analytes in mobile phase at 10 μL/min using Analyst 1.6.2 software tuning module. The Q1/Q3 (m/z) transitions monitored: 363/147 (D2HG) and 367/151 (L/D-2HG-d4).

Calibration and quantification—A set of calibrator samples in NeuroCult NSC base media was prepared by adding appropriate amounts of pure D2HG at the following concentration levels: 0, 0.032, 0.16, 0.8, 4, and 20 μg/mL. Calibration samples were analyzed alongside the experimental samples and accuracy acceptance criteria was 85% for each but the lowest level (0.032 μg/mL, 80%, LLOQ). The obtained calibration curve was linear (r^2=0.999). Analyst 1.6.2 software was used for integration of the chromatograms, calibration curve calculation, and quantification of the study samples.

RNAi-mediated Knockdown and Transgenic Rescue of GDH1/2

Lentiviral particles containing GDH1/2 targeting shRNA (MISSION catalog: TRCN0000220866) and non-targeting control were generated by the Duke University Functional Genomics RNAi Core Facility. ~1×10^5 patient-derived glioma cells were seeded onto laminin-coated cell culture dishes and allowed to adhere overnight. 16 hours after

seeding, cells were washed and fresh NSC proliferation media was added containing lentiviral particles at 10 MOI. 24 hours later, viral particle containing supernatant was removed and cells were washed twice with neurobasal medium and fresh NSC proliferation media was added. Knockdown was confirmed by western blotting with an anti-GDH1/2 antibody (Cell Signaling Technology #12793). Synthetic cDNA constructs coding for human GDH1 or human GDH2 were custom ordered from GeneWiz, with the codons targeted by the GDH1/2 shRNA synonymously mutated to create shRNA-resistant cDNAs. cDNAs were cloned into the MIGR1 retroviral expression system and delivered into the 08-0537 patient-derived glioma line as described for the murine NSC transgenic lines.

IHC Analysis of Mouse Tumors

Standard H&E procedures were performed requiring paraffin sections to undergo deparaffinization in 3 washes with Sub-X, followed by rehydration of the tissue in a graded Ethanol series, Hematoxylin staining, wash with Ammonia water, Eosin staining, dehydration in a graded Ethanol series, and a clearing in Sub-X followed by mounting with a Sub-X based mounting media. The Duke University Pathology Research Histology and Immunohistochemistry Laboratory was used for processing and staining samples for IHC. A standard protocol was followed and required antigen retrieval in citrate buffer (pH 6.0, 80° Celsius). The DAKO Autostainer 3400 was used with antibodies anti-Ki67 1:100 (BD Pharm-550609), and anti-Olig2 1:500 (Abcam-ab136253). H&E and IHC samples were imaged using the Leica DMD 108.

Statistical Analyses

Comparisons between two groups were evaluated using a t-test (parametric) for experimental cell-based data or Mann-Whitney U test (non-parametric) analyses for TCGA RNA-Seq data. Comparisons of three or more groups were performed by analysis of variance (ANOVA) with multiple comparisons to experimental controls and adjusted for multiplicity by the Bonferonni method. Mantel Cox logrank tests were used to compare survival of animal groups over time. Multiplicity adjusted p-values are reported as *$p<0.05$, **$p<0.01$, ***$p<0.001$.

RESULTS

$IDH1^{R132H}$ expression prolongs survival in a mouse model of glioma

To study the role of heterozygous $IDH1^{R132H/WT}$ mutations in gliomagenesis and brain tumor metabolism, we generated a conditional $IDH1^{R132H}$ knock-in mouse model in which one WT *IDH1* allele is genetically engineered to contain a loxP-STOP-loxP cassette with a neomycin selection marker between exons 2 and 3 of the *IDH1* gene and a two nucleotide substitution (CGA→CAC) at codon 132 to generate the $IDH1^{R132H}$ mutation (Supplemental Figure 1A) (29). In the presence of Cre recombinase, the STOP cassette is excised, thus permitting transcription of the full-length mutant *IDH1* gene in a heterozygous context with WT *IDH1*. Heterozygous $IDH1^{flox/WT}$ mice were crossed with homozygous $TP53^{flox/flox}$ (conditional knockout) animals to better model the genetics of grade II-III astrocytomas and secondary GBM, in which the vast majority of patients with *IDH1* or *IDH2* mutations also harbor loss-of-function mutations or genetic deletions of *TP53* (22,25,31,32).

We first sought to use the genetically engineered mice to generate neural progenitor cell (NPC) lines for studying the effects of $IDH1^{R132H}$ on gliomagenesis. $TP53^{flox/flox}$-$IDH1^{flox/WT}$ male and female mice were crossed and NPCs were harvested from forebrains of E14.5 embryos to generate NPC lines of the genotypes $IDH1^{flox/WT}$-$TP53^{flox/flox}$ and $IDH1^{WT/WT}$-$TP53^{flox/flox}$. After harvesting, the NPCs were cultured for approximately 48 hours in neural stem cell proliferation media and began to form small neurospheres. The NPCs were passaged into fresh neural stem cell media containing an adenovirus vector for delivering and expressing Cre-recombinase (Cre). Adenovirus-mediated delivery of Cre efficiently induced recombination of the floxed genes, thus generating engineered NPCs that were functionally $IDH1^{R132H/WT}$-$TP53^{-/-}$ and $IDH1^{WT/WT}$-$TP53^{-/-}$ (Supplemental Figure 1B).

Previous studies reported that robust gliomagenesis requires both tumor suppressor inactivation and oncogene expression (33,34). We therefore used a retroviral delivery system to express a platelet-derived growth factor-B (PDGF)-IRES-GFP transgene in the isolated NPCs. The PDGF-expressing $IDH1^{R132H/WT}$-$TP53^{-/-}$ and $IDH1^{WT/WT}$-$TP53^{-/-}$ NPCs retained properties of stem-like phenotype after virus-mediated delivery of both Cre and PDGF, as indicated by nestin expression (Supplemental Figure 1C) and neurosphere formation after serial passages.

To investigate the gliomagenic potential of these engineered NPCs, as well as the role of heterozygous $IDH1^{R132H/WT}$ mutation, the NPCs were expanded in cell culture as neurospheres and then transplanted into the right caudate nucleus of NOD-SCID-γ (NSG) mice. Transplantation of $TP53^{-/-}$ NPCs with transgenic overexpression of PDGF ("gliomagenic progenitor cells," GPCs) generated brain tumor symptoms that required animal euthanasia in both $IDH1^{WT/WT}$ and $IDH1^{R132H/WT}$ conditions (Figure 1A). However, the onset of symptoms was significantly delayed for animals with $IDH1^{R132H/WT}$ tumors (Figure 1B) ($p=.02$). H&E staining revealed that $IDH1^{WT/WT}$ tumors appeared generally more diffuse and invasive than $IDH1^{R132H/WT}$ tumors, while $IDH1^{R132H/WT}$ tumors exhibited more defined tumor borders. (Figure 1C). We performed immunohistochemical staining of $IDH1^{WT/WT}$ and $IDH1^{R132H/WT}$ mouse brain tumors, derived from transplanted GPCs, to further evaluate $IDH1^{R132H}$-dependent differences between the tumors (Figure 1C, Supplemental Figure 1D). Both groups showed Olig2-positive staining throughout the tumor. Additionally, both $IDH1^{WT/WT}$ and $IDH1^{R132H/WT}$ tumors contained a high percentage of Ki67-positive cells (staining index of 30–90%), indicating that the tumors were high-grade and highly proliferative at the time animals were euthanized due to symptoms.

Transgenic expression of $IDH1^{R132H}$ significantly decreased murine GPC proliferation in cell culture relative to a vector-transduced control line (Figure 1D), raising the possibility that $IDH1^{R132H}$ therapeutic inhibition alone may not be an ideal strategy for limiting the growth of these cells. To evaluate the effects of an $IDH1^{R132H}$ small-molecule inhibitor on a patient-derived cell line, we treated a patient-derived $IDH1^{R132H/WT}$ secondary GBM stem-like cell line with AGI-5198, a potent and specific inhibitor of $IDH1^{R132H}$ neomorphic enzyme activity (12). AGI-5198 treatment significantly inhibited the production of D2HG

(Figure 1E) but failed to inhibit growth of 08-0537 cells over an 8-day timecourse (Figure 1F).

IDH1^{R132H} expression decreases TCA cycle metabolites and slows cell growth

The differences observed in tumor progression (Figure 1B) and GPC proliferation (Figure 1D) suggested that IDH1$^{R132H/WT}$ expression may be sufficient to decrease gliomagenic cell growth. Previous results from our laboratory and others have reported that IDH1^{R132H} expression causes widespread metabolic reprogramming (13,15,16), which is likely to slow glioma growth in the absence of compensatory metabolic mechanisms. To evaluate the metabolic effects of IDH1^{R132H} expression in our GPC models, we first used PDGF-IDH1$^{WT/WT}$-TP53$^{-/-}$ GPCs transduced with empty vector or expressing IDH1^{WT} or IDH1^{R132H} (Supplemental Figure 2A) and measured metabolite abundance using a quantitative metabolomics platform. This approach was selected in favor of using IDH1$^{flox/WT}$-TP53$^{flox/flox}$ NSCs (+/− Cre) because the selected approach allowed evaluation of IDH1^{WT} or IDH1^{R132H} expression with coincident deletion of *TP53* deletion in all conditions.

Quantitative metabolomics analysis revealed that IDH1^{R132H} expression caused a significant, expected increase in D2HG relative to IDH1^{WT} and empty vector controls (Figure 2A). Additionally, IDH1^{R132H} expression caused a significant decrease in critical TCA cycle metabolites, including aconitate, citrate, fumarate, and malate (Figure 2B–2G, Supplemental Figure 2B). Glutamine levels were reduced in IDH1^{R132H}-expressing cells, while glutamate levels were unchanged (Figures 2H, 2I). A summary of IDH1^{R132H}-dependent effects on TCA cycle metabolites and glutamine anaplerosis can be found in Figure 2J. Additionally, the abundance of numerous dipeptide metabolites was significantly increased in IDH1^{R132H} expressing cells (Figure 2K, 2L), suggesting that these cells have increased proteolytic protein turnover or increased uptake of extracellular dipeptides relative to IDH1^{WT} cells (Supplemental Dataset A). Collectively, these results revealed that IDH1^{R132H} expression decreases a number of critical macromolecule precursor metabolites within the TCA cycle.

Adaptive substitutions in the GDH2 allosteric domain confer a growth advantage in IDH1$^{R132H/WT}$ GPCs

IDH1^{R132H}-expressing cells are reported to have an increased reliance on the glutaminolytic flux of glutamine and glutamate to lipids via the TCA cycle (14,16,18). Because IDH1^{R132H} expression slowed murine glioma growth in vivo and decreased TCA cycle metabolite abundance in GPCs (Figure 1B, 2J), we examined the TCGA low-grade glioma (TCGA-LGG) dataset to determine whether human gliomas compensate for mutant IDH1/2-induced metabolic changes by altering the expression of enzymes involved in glutaminolysis (31). We specifically examined expression of glutaminase (GLS), glutamate dehydrogenase 1 (GDH1), and glutamate dehydrogenase 2 (GDH2), and compared mRNA expression of these genes between patients bearing tumors with *IDH1* or *IDH2* mutations vs. *IDH1/2* wild-type patients using freely available RNA-Seq data in the TCGA-LGG database. GLS mRNA expression was not significantly different between *IDH1/2* mutant and *IDH1/2* wild-type cases (Figure 3A). However, both GDH1 and GDH2 mRNA expression was significantly

elevated in the tumors of patients with *IDH1/2* mutations compared to *IDH1/2* wild-type patients (Figure 3B, 3C). This result is consistent with a previous report of increased GDH1/2 mRNA expression in GBM cases with *IDH1/2* mutations compared to *IDH1/2* wild-type cases (15). Further examination of specific histological tumor subsets of the TCGA-LGG RNA-seq data revealed that GDH2 expression was increased in *IDH1/2* mutant cases in all glioma subsets (i.e. astrocytoma, oligoastrocytoma, oligodendroglioma) (Supplemental Figures 3A–C).

To determine whether GDH1 or GDH2 overexpression could increase the growth of GPCs with $IDH1^{R132H}$ expression, we overexpressed human GDH1 or human GDH2 in $IDH1^{R132H}$-$TP53^{-/-}$ GPCs (Supplemental Figure 4) and examined the extent to which GDH1/2 expression affected neurosphere formation in collagen matrix. It is important to note that while *GLUD1*, (the gene that encodes GDH1) is an ancestral and ubiquitously expressed gene, *GLUD2* (the gene that encodes GDH2) is only present in hominoid species and is expressed primarily in the reproductive organs and central nervous system (35). Transgenic expression of GDH2, but not GDH1, increased GPC sphere formation in collagen, suggesting that GDH2 provides a non-redundant, growth-promoting function relative to human GDH1 (Figure 3D). Both high glucose and low glucose conditions were evaluated based on a previous study that reported IDH mutant-expressing cells were sensitive to epigallocatechin-3-gallate (EGCG, a putative GDH inhibitor) and a pan-transaminase inhibitor only under low-glucose cell culture conditions (18). However, we observed a GDH2-dependent increase in sphere formation under both conditions.

The *GLUD2* gene was formed by a retroduplication of the *GLUD1* gene in a hominoid ancestor, and the GDH1 and GDH2 proteins are highly similar, with ~96% sequence identity. However, recently evolved amino acid substitutions in GDH2 (Supplemental Figure 5) have been reported to alter mitochondrial localization (36) and confer markedly different allosteric properties that facilitate glutamate metabolism in the human brain (26–28,36).

Based on the recently evolved amino acid substitutions in GDH2 (relative to GDH1) and a published report suggesting differential subcellular localization (36), we investigated the extent to which mitochondrial localization of GDH1 and GDH2 differed in a patient-derived $IDH1^{R132H/WT}$ secondary GBM cell line. Commercial antibodies cannot distinguish GDH1 vs. GDH2 protein by immunodetection methods. We therefore synthesized shRNA-resistant GDH1 and GDH2 cDNAs in which the shRNA-targeted codons were synonymously mutated in order to prevent RNAi-mediated targeting of the transgenic mRNAs. We then used these shRNA-resistant cDNAs to rescue GDH1 or GDH2 expression in 08-0537 cells that were expressing GDH1/2-targeting shRNA. Using confocal microscopy and immunofluorescence, we observed that GDH1 and GDH2 displayed similar co-localization with the mitochondrial marker cytochrome C (Figure 3E, Supplemental Figure 6). Because we observed that GDH1 and GDH2 display similar subcellular localization in the $IDH1^{R132H/WT}$ brain tumor stem-like cell line under study, we hypothesized that a mechanism distinct from altered subcellular localization or mitochondrial targeting was responsible for the GDH2-specific growth-promoting properties observed in Figure 3D.

Next, we investigated the extent to which two specific amino acid substitutions in the GDH2 allosteric domain regulate GPC growth. Evolutionary substitutions in the GDH2 allosteric domain (Ser^{496} and Ala^{509}) have conferred unique enzymatic properties to GDH2, including a lower optimal pH, resistance to GTP-mediated inhibition, and ADP-dependent activation relative to GDH1 (Figure 3F) (27,37,38). We hypothesized that if the GDH2-dependent growth advantage of $IDH1^{R132H}$-expressing GPCs involved these evolutionary adaptations, then mutating Ser^{496} and Ala^{509} back to the corresponding amino acids in GDH1 would inhibit growth of $IDH1^{R132H/WT}$ cells (Supplemental Figure 5). Using our murine GPC model system (Figure 3G), only GDH2 expression caused a significant increase in GPC growth over 4 days in culture (Figure 3H) relative to cells expressing transgenic GDH1 or the allosteric domain mutants $GDH2^{S496R}$ and $GDH2^{A509G}$.

Glutamate Dehydrogenase 2 rescues $IDH1^{R132H}$-induced metabolic liabilities in gliomagenic progenitor cells

To investigate the metabolic mechanisms underlying the GDH2-dependent increase in $IDH1^{R132H}$-$TP53^{-/-}$ GPC growth, we performed a quantitative metabolomics analysis of PDGF-$IDH1^{R132H/WT}$-$TP53^{-/-}$ GPCs expressing empty vector, GDH1, or GDH2 (Supplemental Figure 7). When compared to the empty vector condition, human GDH1 and GDH2-expressing GPCs exhibited significant and/or trending decreases in glucose and several glycolytic intermediates (glucose 6-phosphate, fructose-6-phosphate, isobaric compound fructose 1,6-diphosphate, 3-phospholglcyerate, and phosphoenolpyruvate) (Figure 4A–G). Decreases were also apparent in metabolites generated from glucose 6-phosphate and fructose 6-phosphate via the pentose phosphate pathway and sorbitol pathways (e.g., 6-phosphogluconate and fructose) (Supplemental Dataset B).

GDH1 or GDH2 expression did not significantly alter D2HG abundance in GPCs (Figure 5A). GDH2-expressing GPCs exhibited significant increases in several early stage TCA cycle intermediates (Supplemental Figure 8), including citrate, aconitate, and α-ketoglutarate (the product of the GDH2 reaction) (Figure 5B–5D). Succinate was significantly decreased in GDH1-expressing cells, while fumarate and malate levels were not affected by GDH expression (Figure 5E–G). The observed changes in TCA cycle metabolites are indicative of altered flow through the cycle, and may have arisen in part from increased uptake and utilization of glutamine and glutamate in GDH2-expressing cells. Consistent with this hypothesis, GDH2 expression caused an increase in the abundance of intracellular glutamate but did not alter glutamine levels (Figure 5H–I). A summary of GDH2-dependent effects on TCA cycle metabolites and glutamine anaplerosis can be found in Figure 5J.

Transgenic expression of GDH2, but not GDH1, reversed the $IDH1^{R132H}$-dependent increases in dipeptide metabolites (Figure 6A) and caused a significant increase in γ-glutamyl amino acids (Figure 6A, Supplemental Dataset B), metabolites that play an important role in amino acid transport and glutathione recycling. Notably, GDH2 expression increased the abundance of intracellular γ-glutamylglutamate and γ-glutamylglutamine (Figure 6B–C), but did not alter the abundance of γ-glutamylcysteine or glutathione metabolites (Figure 6D–F), suggesting that GDH2 expression in GPCs may stimulate amino

acid uptake for glutamate-dependent TCA cycle anaplerosis, rather than promoting increased glutathione biosynthesis (Figure 6G).

GDH2 allosteric domain confers a growth advantage in orthotopic mouse models of IDH1$^{R132H/WT}$ glioma

Results from the GPC sphere formation assay, metabolomics analyses, and GPC proliferation assay demonstrated that GDH2 expression confers a non-redundant, growth-promoting effect in IDH1^{R132H}-expressing GPCs in a manner that requires allosteric domain substitutions that are specific to GDH2 (Figures 3, 5, 6). Therefore, we sought to determine whether GDH2 and GDH2-specific allosteric amino acid substitutions confer accelerated growth and enhanced tumorigenicity in two orthotopic models of IDH1$^{R132H/WT}$ glioma. First, we expressed GDH1, GDH2, GDH2^{S496R}, or GDH2^{A509G} transgenes in the 08-0537 cell line (Figure 7A). 08-0537 is gliomagenic in nude mice with a latency of ~30 days (Supplemental Figure 9). 08-0537 transgenic cell lines were orthotopically transplanted into the right caudate nucleus of nude mice and mice were monitored for the onset of neurological symptoms. GDH1/2 dual knockdown caused a significant increase in median survival (80 days) relative to the control condition (33 days) (Figure 7B, Supplemental Figure 10). Transgenic expression of GDH2 in GDH1/2 knockdown cells (GDH2 rescue) significantly accelerated the onset of symptoms in tumor-bearing animals (median survival: 40 days) relative to the GDH1/2 knockdown condition. Expression of GDH1, GDH2^{S496R}, or GDH2^{A509G} transgenes also shortened animal survival relative to the GDH1/2 knockdown condition. However, these animals survived significantly longer than the shControl condition, whereas GDH2-expressing animals did not (Figure 7B, Supplemental Figure 10).

Next, we tested the tumorigenicity of GPCs infected with empty vector (expressing only murine Gdh1) or GDH2 (expressing both murine Gdh1 and human GDH2) by transplanting these GPC lines into NSG mice and euthanizing the mice at exactly 30 days post-transplantation. Notably, one animal in the GDH2 group was symptomatic on day 30 (weight loss, inability to ambulate), while none of the animals in the control group exhibited symptoms. Histological and immunohistochemical examination of the right caudate nucleus of the animals revealed a striking increase in the abundance of proliferative cells (Ki67+) and Olig2+ cells in the GDH2 group relative to the control group (Figure 7C), demonstrating that GDH2 expression is sufficient to accelerate gliomagenesis in IDH1$^{R132H/WT}$ GPCs.

Discussion

The overall objective of this study was to investigate the effect of *IDH1* mutations on gliomagenesis and brain tumor metabolism and to identify potential compensatory metabolic alterations that promote glioma growth in the context of *IDH1* mutations. Using murine neural stem cells as a model system, we found that IDH1^{R132H} expression induces growth-limiting metabolic alterations, which inhibit the growth of murine gliomas in vivo (Figure 1B) and gliomagenic NPCs in vitro (Figure 1D). Expression of GDH2 altered a number of IDH1^{R132H}-induced metabolic changes, including the rescue of specific TCA metabolites (citrate, aconitate, and αKG) and a reversal of IDH1^{R132H}-dependent perturbations on

dipeptide and γ-glutamyl amino acid metabolism (Figure 5J, 6G). GDH2-dependent metabolic changes coincided with increased GPC proliferation in vitro (Figure 3H) and increased gliomagenesis and accelerated glioma growth in vivo (Figure 7B, 7C). Importantly, the growth advantage of GDH2-expressing NSCs and xenografts was largely dependent on evolutionary amino acid substitutions in the GDH2 allosteric domain (Figure 3H, 7B).

GDHs are ancient enzymes that catalyze the oxidative deamination of glutamate to generate αKG. Ancestral forms of GDH enzymes are primarily regulated at the level of transcription and are not susceptible to allosteric regulation (39). Ciliates evolved a GDH "antenna" domain that allowed the enzyme to be regulated by ADP and fatty acids (40) (Figure 3F). Subsequently, the GDH1 enzyme further evolved in mammals to become susceptible to numerous allosteric regulators, including GTP, l-leucine, and l-isoleucine (40). The *GLUD1* gene was retroduplicated to the X-chromosome in a hominoid ancestor ~23 million years ago to form the intronless *GLUD2* gene (26). After retroduplication, a period of rapid evolutionary adaptation conferred markedly different allosteric properties to GDH2 that may facilitate glutamate turnover in the human brain (26–28,36) (Supplemental Figure 5). Specifically, the GDH2 allosteric domain contains at least two functional amino acid substitutions, R496S and G509A. The R496S substitution renders GDH2 activity ADP-inducible and lowers the optimal pH for enzymatic activity to ~7.0, and the G509A substitution makes GDH2 resistant to GTP-mediated inhibition. Given the observed importance of GDH2 Ser^{496} and Ala^{509} to glioma progression and cell proliferation (Figure 3, 7), it is possible that $IDH1^{R132H}$-dependent D2HG production suppresses GDH1 activity, while GDH2 activity is maintained by these adaptive allosteric substitutions.

Glutamate is an abundant neurotransmitter in the human brain (41), and it has been suggested that the increased uptake and turnover of glutamate during neurotransmission may bypass the need for glutaminase activity and provide an alternative carbon source for biosynthetic pathways in *IDH1* mutant gliomas (42). In our genetically engineered murine GPCs, we observed that GDH2 expression, but not GDH1 expression, increased the abundance of γ-glutamyl amino acids, as well as intracellular glutamate and αKG, but did not elicit a concomitant increase in glutathione metabolites (Figure 6). This result raises the possibility that *IDH1/2* mutant gliomas increase the uptake of amino acids from the extracellular environment, including the neurotransmitter glutamate, in a manner that requires γ-glutamyl transferases (GGTs), which are reported to be highly expressed in WHO grade III astrocytomas and GBM (43). Increased uptake of γ-glutamylglutamate and γ-glutamylglutamine via GGTs may also provide an explanation for the elevated levels of intracellular glutamate that were observed specifically in cells expressing GDH2 (Figure 6B–C). An important implication of this result is that it may provide support for the hypothesis that *IDH1/2* mutant gliomas preferentially occur in the forebrain due to high glutamate flux. According to this hypothesized model, the increased uptake and utilization of extracellular amino acids (specifically, glutamate) may provide a critical carbon source that compensates for altered αKG flux in $IDH1^{R132H}$, and our results suggest that this process occurs in a GDH2-dependent manner.

Several recent studies have reported that GDH enzymes promote growth of tumor cells from various tissues (15,44,45). One of these studies investigated the distinct actions of GDH1 and GDH2, and found that only GDH2 overexpression reversed deficiencies in anaplerotic glutamine flux that were caused by expression of an $IDH1^{R132H}$ transgene (15). This finding is consistent with our metabolomics studies, which showed a GDH2-dependent rescue of αKG, cis-aconitate, and citrate in heterozygous $IDH1^{R132H/WT}$ GPCs (Figure 6), although we also observe that GDH2 expression causes a general decrease in glycolytic metabolites, suggesting a possible suppression of glycolytic flux in this context (Figure 5). Additionally, the previous study by Chen et al. also reported that dual knockdown of GDH1/2 by RNAi decreased tumor cell density in a hemizygous $IDH1^{R132H/-}$ glioma xenograft (15), and we now show that targeting GDH2 is likely sufficient for growth inhibition of a patient-derived heterozygous $IDH1^{R132H/WT}$ GBM xenograft (Figure 7B). Although the murine NSC and murine glioma results clearly demonstrate that GDH2 confers a growth-promoting effect in the context of $IDH1^{R132H}$ expression (Figure 4, 7) (15), it is important to note that the results from our $IDH1^{R132H/WT}$ xenograft experiment cannot rule out the possibility that GDH1 expression plays a role in the $IDH1^{R132H}$ glioma growth, as GDH1 rescue induced a partial decrease in animal survival (Figure 7B).

By identifying the specific GDH2 domain that promotes IDH-mutant glioma growth, our results raise several notable issues related to drug-targeting and glioma therapy. First, while GDH1 is an ubiquitously expressed housekeeping enzyme, current evidence suggests that GDH2 expression is restricted to the brain, reproductive organs, and kidneys (46). The relatively restricted tissue expression of GDH2, coupled with its non-redundant glioma-promoting function, suggests that GDH2-specific inhibition may provide a therapeutic advantage by sparing the housekeeping functions of GDH1. Additionally, the functional differences in GDH1 and GDH2 are mediated, in part, by functional substitutions in the allosteric domain (Figure 4, 7) (27), and our results demonstrate, in principle, that pharmacological approaches for targeting GDH2-specific allostery are feasible from a therapeutic perspective.

Finally, while the therapeutic benefit of targeting *IDH1/2* mutations is relatively clear in the context of leukemia therapy (47), the potential benefit of targeting mutant IDH enzymes in glioma is not yet established. An important implication of the results of our study is that pharmacological targeting of mutant IDH1 neomorphic activity per se may not be sufficient to inhibit or slow growth of IDH mutant tumor cells. This finding is consistent with several recent studies that demonstrated that exploiting $IDH1^{R132H}$-dependent sensitivities, rather than direct inhibition of neomorphic enzyme activity, may be a superior strategy for inhibiting growth of solid tumors with IDH1 mutations. Tateishi et al. recently reported that D2HG depletion, via mutant IDH1 inhibition, did not inhibit cell growth in malignant glioma cell lines and did not slow the propagation of a orthotopic glioma xenograft in a mouse model (48). Instead, the investigators found that the continued action of IDH1 mutant activity induced a metabolic sensitivity that could be exploited by inhibiting nicotinamide phosphoribosyltransferase (NAMPT), an enzyme involved in the NAD+ salvage pathway. Similarly, Sulkowski et al. reported that D2HG produced by mutant IDH1 causes a defect in double-strand break repair by homologous recombination and thus induces a sensitivity to poly (ADP–ribose) polymerase (PARP) inhibitors (49). Another group reported that

inhibiting PARP-mediated DNA repair pathways sensitized IDH1 mutant glioma cells to temozolomide treatment (50). Additionally, Johannessen et al. used immortalized astrocytes expressing $IDH1^{R132H}$ to find that, although IDH1 mutation drives the transformation of immortalized astrocytes, the mutant IDH1 inhibitor AGI-5198 does not reverse histone hypermethylation or inhibit cell growth in cells that have already undergone $IDH1^{R132H}$-mediated transformation. Consequently, it is important to consider whether the clinical use of IDH1 mutant inhibitors, specifically in solid tumors, may ablate potential metabolic or PARP-inhibitor sensitivities. Our results provide an evidence-based alternative strategy for targeting $IDH1^{R132H}$ expression in gliomas. Rather than directly targeting the neomorphic activity of $IDH1^{R132H}$, our results have established the feasibility of targeting $IDH1^{R132H}$-induced metabolic liabilities by inhibiting GDH2.

Supplementary Material

Refer to Web version on PubMed Central for supplementary material.

Acknowledgments

Grant Support: H. Yan received NIH R01 grants R01CA140316 and R01NS096407. H. S. Friedman received the institutional training grant T32CA074736. M. S. Waitkus was supported by NIH T32CA074736.

We thank Paula Greer and Huishan Zhou for technical assistance.

References

1. Paschka P, Schlenk RF, Gaidzik VI, Habdank M, Krönke J, Bullinger L, et al. IDH1 and IDH2 mutations are frequent genetic alterations in acute myeloid leukemia and confer adverse prognosis in cytogenetically normal acute myeloid leukemia with NPM1 mutation without FLT3 internal tandem duplication. J Clin Oncol. 2010; 28:3636–43. [PubMed: 20567020]
2. Borger DR, Tanabe KK, Fan KC, Lopez HU, Fantin VR, Straley KS, et al. Frequent Mutation of Isocitrate Dehydrogenase (IDH)1 and IDH2 in Cholangiocarcinoma Identified Through Broad-Based Tumor Genotyping. Oncologist. 2012; 17:72–9. [PubMed: 22180306]
3. Amary MF, Bacsi K, Maggiani F, Damato S, Halai D, Berisha F, et al. IDH1 and IDH2 mutations are frequent events in central chondrosarcoma and central and periosteal chondromas but not in other mesenchymal tumours. J Pathol. 2011; 224:334–43. [PubMed: 21598255]
4. Parsons DW, Jones S, Zhang X, Lin JC-H, Leary RJ, Angenendt P, et al. An integrated genomic analysis of human glioblastoma multiforme. Science. 2008; 321:1807–12. [PubMed: 18772396]
5. Yan H, Parsons DWW, Jin G, McLendon R, Rasheed BAA, Yuan W, et al. IDH1 and IDH2 mutations in gliomas. N Engl J Med. 2009; 360:765–73. [PubMed: 19228619]
6. Kang MR, Kim MS, Oh JE, Kim YR, Song SY, Seo S II, et al. Mutational analysis of IDH1 codon 132 in glioblastomas and other common cancers. Int J Cancer. 2009; 125:353–5. [PubMed: 19378339]
7. Dang, L., White, DW., Gross, S., Bennett, BD., Bittinger, Ma, Driggers, EM., et al. Nature. Vol. 462. Nature Publishing Group; 2009. Cancer-associated IDH1 mutations produce 2-hydroxyglutarate; p. 739-44.
8. Duncan CG, Barwick BG, Jin G, Rago C, Kapoor-Vazirani P, Powell DR, et al. A heterozygous IDH1R132H/WT mutation induces genome-wide alterations in DNA methylation. Genome Res. 2012; 22:2339–55. [PubMed: 22899282]
9. Figueroa ME, Abdel-Wahab O, Lu C, Ward PS, Patel J, Shih A, et al. Leukemic IDH1 and IDH2 mutations result in a hypermethylation phenotype, disrupt TET2 function, and impair hematopoietic differentiation. Cancer Cell. 2010; 18:553–67. [PubMed: 21130701]

10. Turcan, S., Rohle, D., Goenka, A., Walsh, La, Fang, F., Yilmaz, E., et al. Nature. Vol. 483. Nature Publishing Group; 2012. IDH1 mutation is sufficient to establish the glioma hypermethylator phenotype; p. 479-83.
11. Lu C, Ward PS, Kapoor GS, Rohle D, Turcan S, Abdel-Wahab O, et al. IDH mutation impairs histone demethylation and results in a block to cell differentiation. Nature Nature Publishing Group. 2012; 483:474–8.
12. Rohle D, Popovici-Muller J, Palaskas N, Turcan S, Grommes C, Campos C, et al. An inhibitor of mutant IDH1 delays growth and promotes differentiation of glioma cells. Science. 2013; 340:626–30. [PubMed: 23558169]
13. Reitman ZJ, Jin G, Karoly ED, Spasojevic I, Yang J, Kinzler KW, et al. Profiling the effects of isocitrate dehydrogenase 1 and 2 mutations on the cellular metabolome. Proc Natl Acad Sci U S A. 2011; 108:3270–5. [PubMed: 21289278]
14. Reitman ZJ, Duncan CG, Poteet E, Winters A, Yan L-JJ, Gooden DM, et al. Cancer-associated Isocitrate Dehydrogenase 1 (IDH1) R132H Mutation and d-2-Hydroxyglutarate Stimulate Glutamine Metabolism under Hypoxia. J Biol Chem. 2014; 289:23318–28. [PubMed: 24986863]
15. Chen R, Nishimura MC, Kharbanda S, Peale F, Deng Y, Daemen A, et al. Hominoid-specific enzyme GLUD2 promotes growth of IDH1R132H glioma. Proc Natl Acad Sci U S A. 2014; 111:14217–22. [PubMed: 25225364]
16. Ohka F, Ito M, Ranjit M, Senga T, Motomura A, Motomura K, et al. Quantitative metabolome analysis profiles activation of glutaminolysis in glioma with IDH1 mutation. Tumour Biol. 2014
17. Emadi A, Jun SA, Tsukamoto T, Fathi AT, Minden MD, Dang CV. Inhibition of glutaminase selectively suppresses the growth of primary acute myeloid leukemia cells with IDH mutations. Exp Hematol ISEH - Society for Hematology and Stem Cells. 2014; 42:247–51.
18. Seltzer MJ, Bennett BD, Joshi AD, Gao P, Thomas AG, Ferraris DV, et al. Inhibition of glutaminase preferentially slows growth of glioma cells with mutant IDH1. Cancer Res. 2010; 70:8981–7. [PubMed: 21045145]
19. Garber K. Cancer anabolic metabolism inhibitors move into clinic. Nat Biotechnol. 2016; 34:794–5. [PubMed: 27504761]
20. Altman, BJ., Stine, ZE., Dang, CV. From Krebs to clinic: glutamine metabolism to cancer therapy. Nat Publ Gr. Nature Publishing Group; 2016.
21. Jin G, Reitman ZJ, Duncan CG, Spasojevic I, Gooden DM, Rasheed BA, et al. Disruption of wild-type IDH1 suppresses D-2-hydroxyglutarate production in IDH1-mutated gliomas. Cancer Res. 2013; 73:496–501. [PubMed: 23204232]
22. Killela PJ, Pirozzi CJ, Reitman ZJ, Jones S, Rasheed BA, Lipp E, et al. The genetic landscape of anaplastic astrocytoma. Oncotarget. 2013
23. Waitkus MS, Diplas BH, Yan H. Isocitrate dehydrogenase mutations in gliomas. Neuro Oncol. 2016; 18:16–26. [PubMed: 26188014]
24. Article O The Cancer Genome Atlas Research Network. Comprehensive, Integrative Genomic Analysis of Diffuse Lower-Grade Gliomas. N Engl J Med. 2015:2481–98.
25. Suzuki H, Aoki K, Chiba K, Sato Y, Shiozawa Y, Shiraishi Y, et al. Mutational landscape and clonal architecture in grade II and III gliomas. Nat Genet Nature Publishing Group. 2015; 47:1–14.
26. Burki F, Kaessmann H. Birth and adaptive evolution of a hominoid gene that supports high neurotransmitter flux. Nat Genet. 2004; 36:1061–3. [PubMed: 15378063]
27. Plaitakis A, Spanaki C, Mastorodemos V, Zaganas I. Study of structure-function relationships in human glutamate dehydrogenases reveals novel molecular mechanisms for the regulation of the nerve tissue-specific (GLUD2) isoenzyme. Neurochem Int. 2003:401–10.
28. Zaganas IV, Kanavouras K, Borompokas N, Arianoglou G, Dimovasili C, Latsoudis H, et al. The odyssey of a young gene: structure-function studies in human glutamate dehydrogenases reveal evolutionary-acquired complex allosteric regulation mechanisms. Neurochem Res. 2014; 39:471–86. [PubMed: 24515454]
29. Pirozzi CJ, Carpenter AB, Waitkus MS, Wang CY, Zhu H, Hansen LJ, et al. Mutant IDH1 Disrupts the Mouse Subventricular Zone and Alters Brain Tumor Progression. Mol Cancer Res. 2017; 15:507–20. [PubMed: 28148827]

30. Struys, Ea, Jansen, EEW., Verhoeven, NM., Jakobs, C. Measurement of urinary D- and L-2-hydroxyglutarate enantiomers by stable-isotope-dilution liquid chromatography-tandem mass spectrometry after derivatization with diacetyl-L-tartaric anhydride. Clin Chem. 2004; 50:1391–5. [PubMed: 15166110]

31. Brat DJ, Verhaak RGW, Aldape KD, Yung WKA, Salama SR, et al. Cancer Genome Atlas Research Network. Comprehensive, Integrative Genomic Analysis of Diffuse Lower-Grade Gliomas. N Engl J Med. 2015; 372:2481–98. [PubMed: 26061751]

32. Eckel-Passow JE, Lachance DH, Molinaro AM, Walsh KM, Decker Pa, Sicotte H, et al. Glioma Groups Based on 1p/19q, *IDH*, and *TERT* Promoter Mutations in Tumors. N Engl J Med. 2015 150610140038004.

33. Hambardzumyan D, Amankulor NM, Helmy KY, Becher OJ, Holland EC. Modeling Adult Gliomas Using RCAS/t-va Technology. Transl Oncol. 2009; 2:89–95. [PubMed: 19412424]

34. Dai C, Celestino JC, Okada Y, Louis DN, Fuller GN, Holland EC. PDGF autocrine stimulation dedifferentiates cultured astrocytes and induces oligodendrogliomas and oligoastrocytomas from neural progenitors and astrocytes in vivo. Genes Dev. 2001; 15:1913–25. [PubMed: 11485986]

35. Zaganas I, Spanaki C, Plaitakis A. Expression of human GLUD2 glutamate dehydrogenase in human tissues: functional implications. Neurochem Int Elsevier Ltd. 2012; 61:455–62.

36. Rosso L, Marques AC, Reichert AS, Kaessmann H. Mitochondrial targeting adaptation of the hominoid-specific glutamate dehydrogenase driven by positive Darwinian selection. PLoS Genet. 2008; 4:e1000150. [PubMed: 18688271]

37. Plaitakis A, Metaxari M, Shashidharan P. Nerve tissue-specific (GLUD2) and housekeeping (GLUD1) human glutamate dehydrogenases are regulated by distinct allosteric mechanisms: Implications for biologic function. J Neurochem. 2000; 75:1862–9. [PubMed: 11032875]

38. Spanaki C, Plaitakis A. The role of glutamate dehydrogenase in mammalian ammonia metabolism. Neurotox Res. 2012; 21:117–27. [PubMed: 22038055]

39. Plaitakis A, Kalef-Ezra E, Kotzamani D, Zaganas I, Spanaki C. The Glutamate Dehydrogenase Pathway and Its Roles in Cell and Tissue Biology in Health and Disease. Biology (Basel). 2017; 6:11.

40. Smith TJ, Stanley Ca. Untangling the glutamate dehydrogenase allosteric nightmare. Trends Biochem Sci. 2008; 33:557–64. [PubMed: 18819805]

41. Schubert F, Gallinat J, Seifert F, Rinneberg H. Glutamate concentrations in human brain using single voxel proton magnetic resonance spectroscopy at 3 Tesla. Neuroimage. 2004; 21:1762–71. [PubMed: 15050596]

42. van Lith, SaM, Navis, AC., Verrijp, K., Niclou, SP., Bjerkvig, R., Wesseling, P., et al. Biochim Biophys Acta. Vol. 1846. Elsevier B.V.; 2014. Glutamate as chemotactic fuel for diffuse glioma cells; are they glutamate suckers?; p. 66-74.

43. Schäfer C, Fels C, Brucke M, Holzhausen HJ, Bahn H, Wellman M, et al. Gamma-glutamyl transferase expression in higher-grade astrocytic glioma. Acta Oncol. 2001; 40:529–35. [PubMed: 11504314]

44. Jin L, Li D, Alesi GN, Fan J, Kang H-B, Lu Z, et al. Glutamate dehydrogenase 1 signals through antioxidant glutathione peroxidase 1 to regulate redox homeostasis and tumor growth. Cancer Cell. 2015; 27:257–70. [PubMed: 25670081]

45. Zhang J, Wang G, Mao Q, Li S, Xiong W, Lin Y, et al. Glutamate dehydrogenase (GDH) regulates bioenergetics and redox homeostasis in human glioma. Oncotarget. 2016

46. Spanaki C, Kotzamani D, Petraki Z, Drakos E, Plaitakis A. Heterogeneous cellular distribution of glutamate dehydrogenase in brain and in non-neural tissues. Neurochem Res. 2014; 39:500–15. [PubMed: 24436052]

47. Stein EM, DiNardo C, Altman JK, Collins R, DeAngelo DJ, Kantarjian HM, et al. Safety and Efficacy of AG-221, a Potent Inhibitor of Mutant IDH2 That Promotes Differentiation of Myeloid Cells in Patients with Advanced Hematologic Malignancies: Results of a Phase 1/2 Trial. Blood American Society of Hematology. 2015; 126:323.

48. Tateishi, K., Wakimoto, H., Iafrate, AJ., Tanaka, S., Loebel, F., Lelic, N., et al. Cancer Cell. Vol. 28. Elsevier Inc; 2015. Extreme Vulnerability of IDH1 Mutant Cancers to NAD+ Depletion; p. 773-84.

49. Sulkowski PL, Corso CD, Robinson ND, Scanlon SE, Purshouse KR, Bai H, et al. 2-Hydroxyglutarate produced by neomorphic IDH mutations suppresses homologous recombination and induces PARP inhibitor sensitivity. Sci Transl Med. 2017; 9:eaal2463. [PubMed: 28148839]

50. Lu Y, Kwintkiewicz J, Liu Y, Tech K, Frady LN, Su YT, et al. Chemosensitivity of IDH1-mutated gliomas due to an impairment in PARP1-mediated DNA repair. Cancer Res. 2017; 77:1709–18. [PubMed: 28202508]

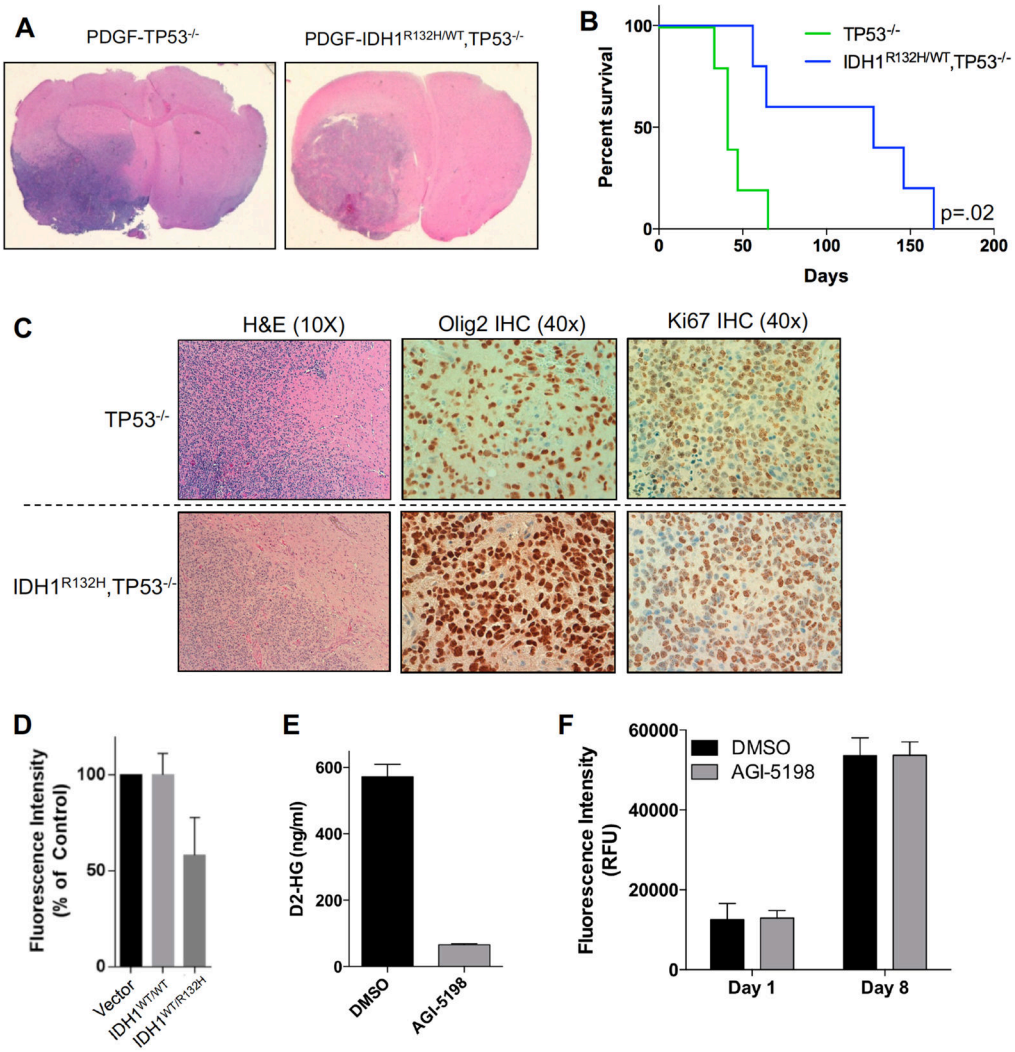

Figure 1. A neural stem cell based murine model of IDH1^{R132H} gliomas

(A) Both IDH1$^{WT/WT}$ and IDH1$^{R132H/WT}$ NSCs generate high-grade gliomas and induce neurological symptoms when transplanted into the right caudate nucleus of NSG mice. (B) Survival curves of mice that received gliomagenic NSC transplantations. N=5 mice were injected and analyzed per group. IDH1$^{R132H/WT}$ had a median survival of 128 days, while the median survival for IDH1$^{WT/WT}$ mice was 41 days (p=.02, Log-Rank test). (C) Representative H&E-stained of IDH1$^{WT/WT}$ and IDH1$^{R132H/WT}$ tumors. Formalin-fixed tissue sections of murine gliomas were stained for tumor markers, including Olig2 and Ki67. IgG staining controls are shown in Supplemental Figure 1. (D) Proliferation of gliomagenic NSCs was assessed by CyQuant assay. 1×10^3 NSCs were seeded onto laminin-coated microplates and allowed to proliferate in low-glucose neural stem cell proliferation media for 4 days. This experiment was performed with 3 independent biological replicates. (E) 5×10^3 08-0537 cells were seeded into 96 well plates, and allowed to adhere overnight. 16 hours after seeding, DMSO or AGI-5198 (5 μM) was added. 48 hours after treatment with DMSO or 5 μM AGI-5198, D2HG abundance in culture media was measured by liquid-chromatography-electron spray ionization-tandem mass spectrometry analysis (F) CyQuant

assay results after 8 days of proliferation in the presence of DMSO control or AGI-5198 (5 μM). Assay was performed using 3 independent biological replicates, each with 4 technical replicate measurements per condition in 96-well plate.

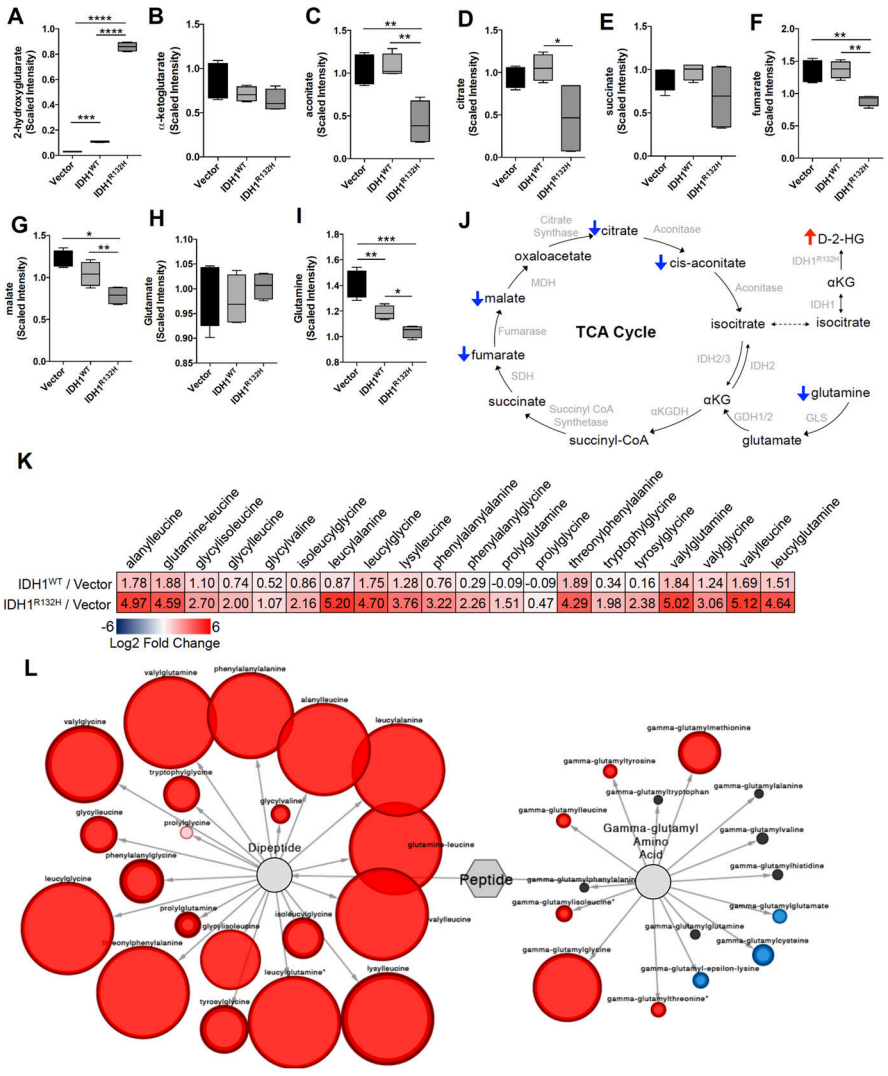

Figure 2. Effects of IDH1^{R132H} on the murine GPC metabolome

(A–I) Metabolite abundance as assessed by LC/MS using the Metabolon Discovery HD4 platform. N=4 samples were cultured, collected, and processed for each condition and metabolite abundance is graphically depicted as scaled intensity (relative abundance). One way analysis of variance and Tukey's post-hoc test was used to evaluate differences between groups, and multiplicity adjusted p-values are reported as *p<0.05, **p<0.01, ***p<0.001. Metabolomics data are available in Supplemental Dataset A as fold changes of group averages. N=4 samples were analyzed for all conditions. (J) Graphical representation of TCA cycle metabolites that are affected by IDH^{R132H} expression in a metabolomics analyses. (K) Table detailing increased abundance of specific dipeptide metabolites in the context of IDH1^{WT} or IDH1^{R132H} transgene expression. The scale bar indicates the log2 fold-change of metabolite abundance relative to the empty vector control condition, with the magnitude of fold change reflected by red or blue color intensity. (L) Pathway analyses of GPC metabolome with IDH1^{R132H} expression relative to the vector control. IDH1^{R132H}-expressing cells showed significant increases in the abundance of dipeptide metabolites, as

well variable differences in the abundance of gamma-glutamyl amino acid metabolites. The changes in metabolite abundance relative to the vector condition are represented by color. Red circles represent increases in metabolite abundance in the $IDH1^{R132H}$-expressing condition and blue circles represent decreases in metabolite abundance in the $IDH1^{R132H}$-expressing condition. The size of the circles is correlated to the magnitude difference in metabolite abundance.

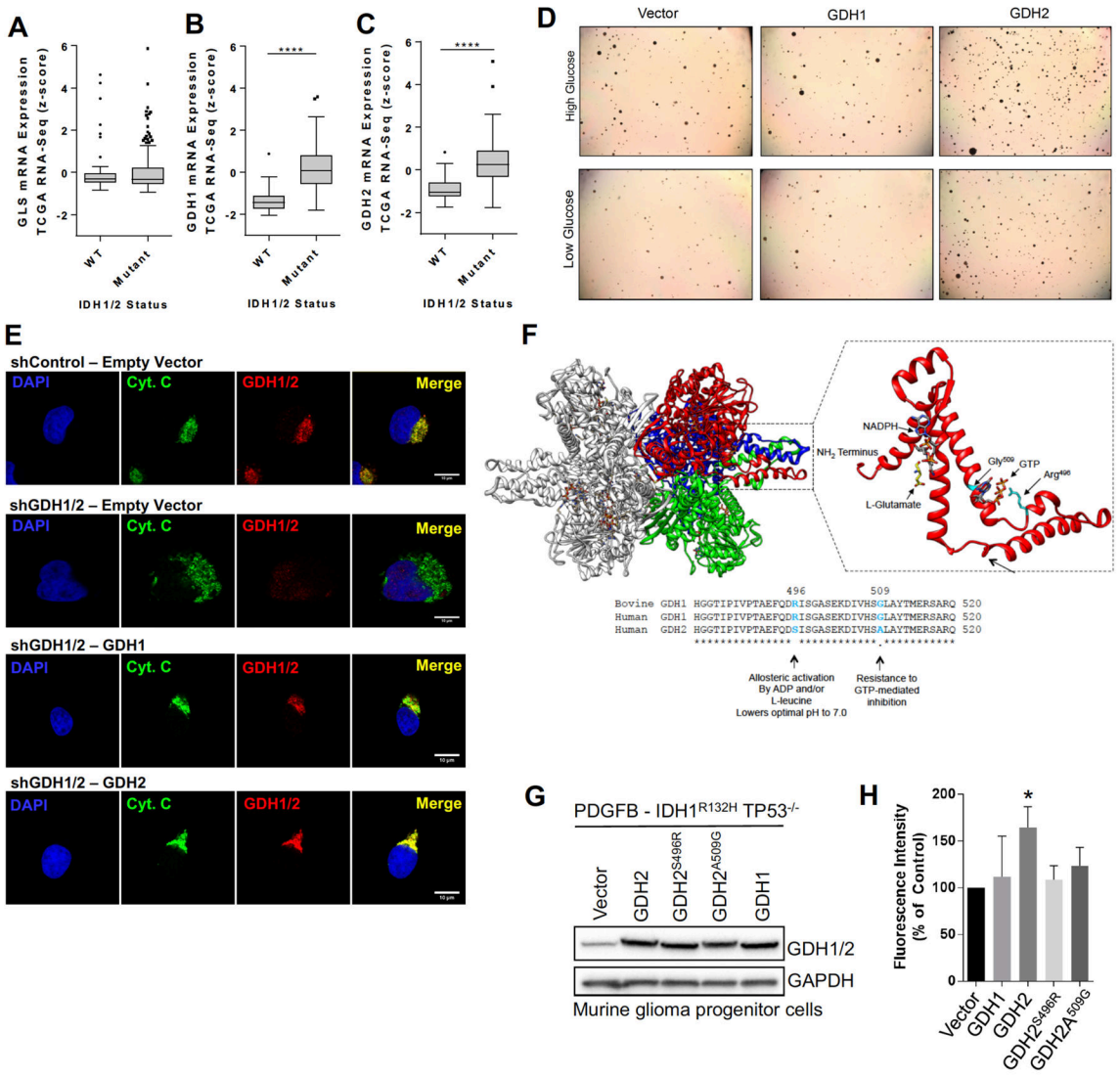

Figure 3. GDH2 expression accelerates the growth of murine GPCs

(A) GLS mRNA expression (z-scores) from the Lower Grade Glioma dataset depicted in Tukey plots and analyzed using a Mann-Whitney U-test. 283 cases with exome sequencing and RNA-seq data were included in the analysis. 52 cases were classified as *IDH1/2*^{WT} and 231 cases harbored mutations in *IDH1 or IDH2*. (B) GDH1 and (C) GDH2 mRNA expression depicted as in (A). (D) Empty vector, GDH1, or GDH2 cDNAs were delivered via retrovirus and expressed in murine gliomagenic NSCs. Sphere-forming potential of gliomagenic NSCs in collagen was assessed in 3 independent biological replicates. (E) Confocal microscopy imaging of 08-0537 cells with variable GDH1/2 expression. Non-targeting or GDH1/2-targeting shRNAs were delivered by lentivirus, and shRNA-resistant cDNAs were subsequently delivered by retrovirus. anti-Cytochrome C staining was used as a mitochondrial marker. DAPI was used as a counterstain. Images were acquired using a 63× oil-immersion objective. (F) Graphical depiction of the hexameric bovine GDH1 crystal structure (PDB ID: 3ETD). 3 subunits are colored in red, green, and blue, and the antenna domain of the red-colored subunit is magnified in the cutout. Binding sites for glutamate and

GTP (allosteric regulator) of GDH1 are shown, and the sites of GDH2 evolutionary substitutions (Arg^{496} and Gly^{509} on GDH1) are shown in cyan. Amino acid sequence alignment shows conservation of amino acids in bovine and human GDH1 in the antenna domain. (G) Western blot analysis of GDH1, GDH2, or GDH2 mutant cDNAs transgenes expressed in murine gliomagenic NSCs after retrovirus-mediated delivery. (H) CyQuant assay results after 4 days of proliferation in low-glucose NSC growth media. Assay was performed using 3 independent biological replicates, each with 4 technical replicate measurements per condition in a 96-well plate.

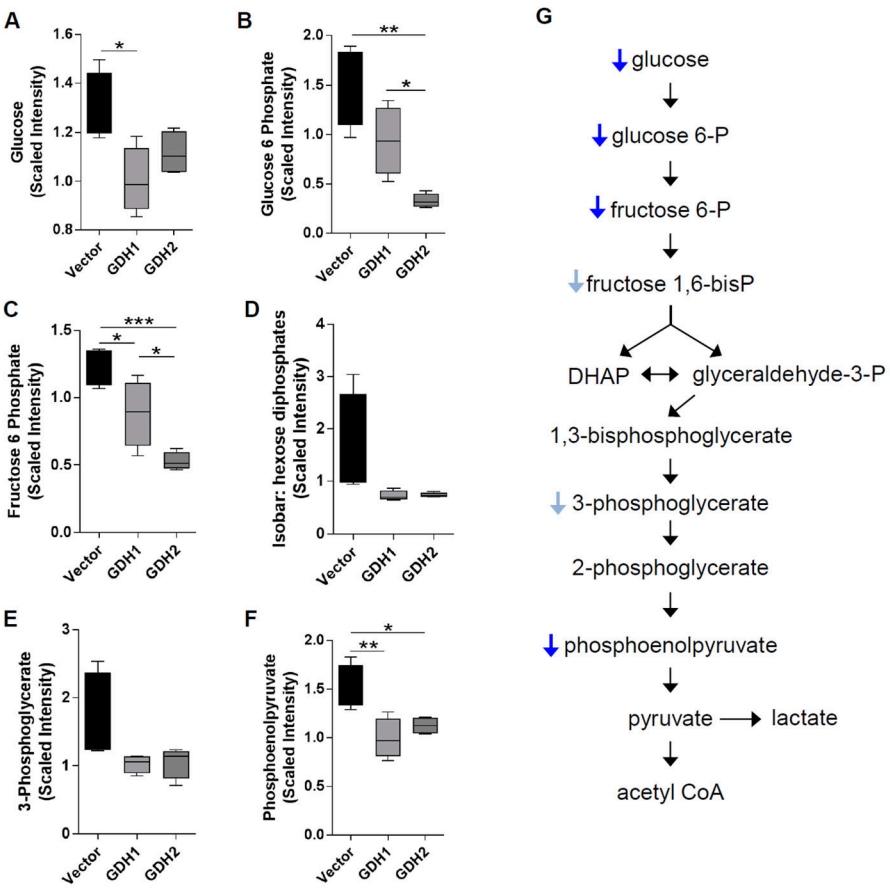

Figure 4. GDH1 and GDH2 transgene expression cause decreased abundance of glycolytic metabolites

(A–F) Expression of GDH1 or GDH2 caused similar, trending decreases in the abundance of glycolytic intermediates relative to the vector control condition, suggesting decreased glycolytic flux in these cells. Trends were similar for both GDH1 and GDH2, although the magnitude of reduction for glucose-6-phosphate and fructose-6-phosphate was greater in the GDH2 condition. Metabolite abundance as assessed by LC/MS using the Metabolon Discovery HD4 platform. N=4 samples were cultured, collected, and processed for each condition and metabolite abundance is graphically depicted as scaled intensity (relative abundance). One way analysis of variance and Tukey's post-hoc test was used to evaluate differences between groups, and multiplicity adjusted p-values are reported as *$p<0.05$, **$p<0.01$, ***$p<0.001$. (G) Graphical depiction of the glycolytic pathway. Statistically significant decreases in metabolites are indicated by dark blue down-arrows, and metabolites that showed trending decreases are indicated by light-blue down-arrows.

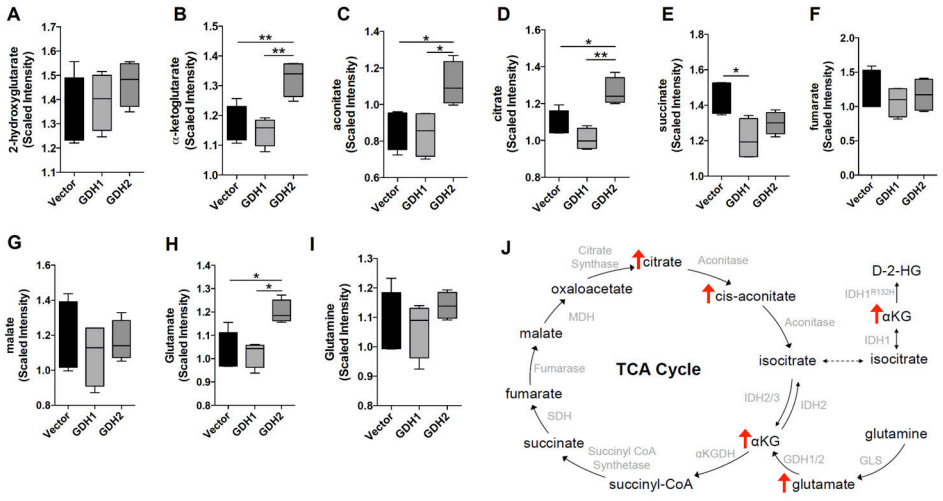

Figure 5. GDH2 expression specifically increases abundance of critical TCA cycle metabolites

(A–I) Metabolite abundance as assessed by LC/MS using the Metabolon Discovery HD4 platform. N=4 samples were cultured, collected, and processed for each condition and metabolite abundance is graphically depicted as scaled intensity (relative abundance). One way analysis of variance and Tukey's post-hoc test was used to evaluate differences between groups, and multiplicity adjusted p-values are reported as *p<0.05, **p<0.01, ***p<0.001. Metabolomics data are available in Supplemental Dataset A as fold changes of group averages. (J) Graphical representation of TCA cycle metabolites that are affected by GDH2 expression in a metabolomics analysis of GDH-expressing GPC lines. N=4 samples were analyzed for all conditions.

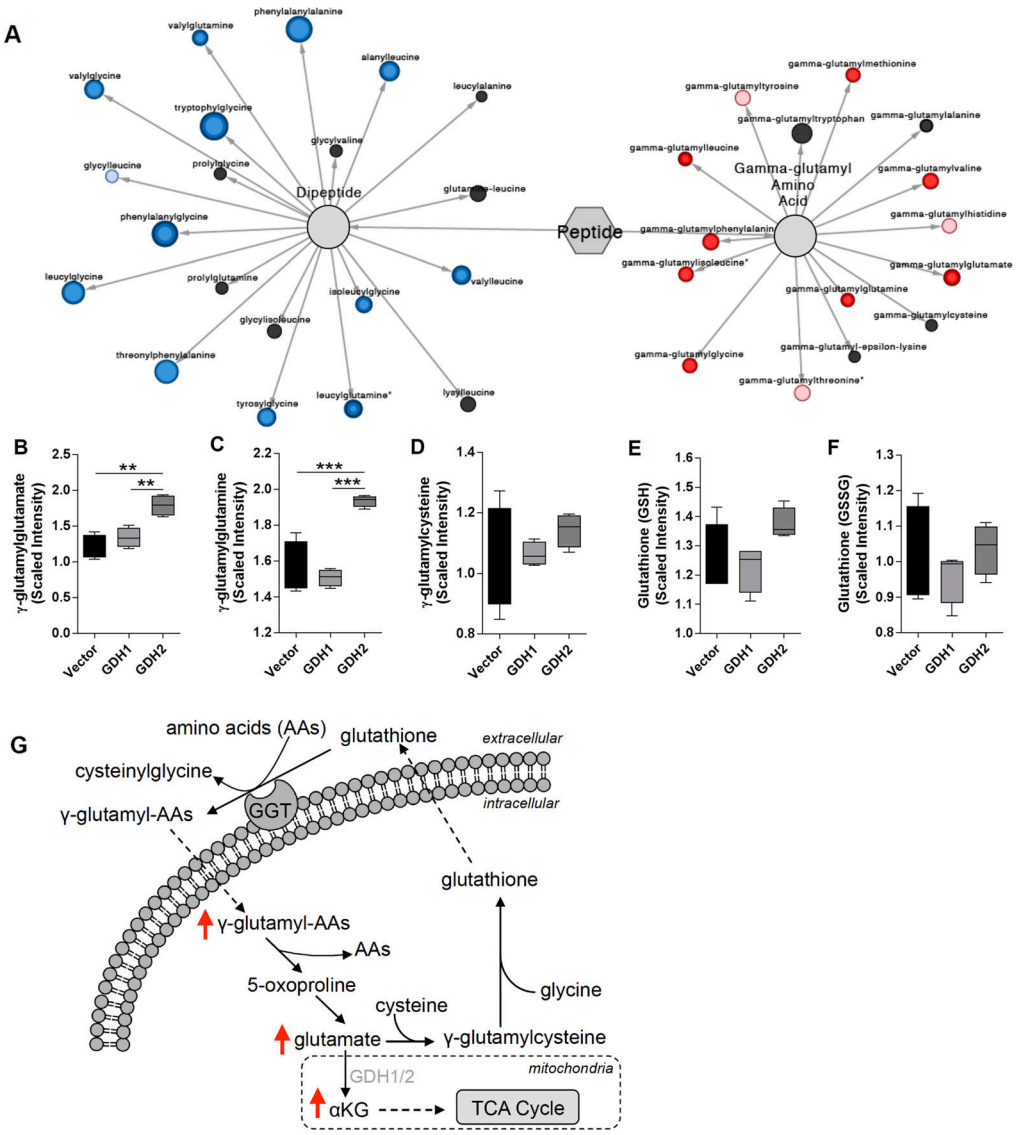

Figure 6. GDH2 expression increases abundance of gamma-glutamyl amino acids

(A) Pathway analyses of NSC metabolome with GDH2 expression relative to the vector control. In contrast to IDH1^{R132H}-mediated effects, GDH2-expressing cells showed significant decreases in the abundance of dipeptide metabolites, as well as increases in the abundance of gamma-glutamyl amino acids. The changes in metabolite abundance relative to the vector condition are represented by color, with red circles representing increases in metabolite abundance in the GDH2-expressing condition and blue circles representing decreases in metabolite abundance in the GDH2-expressing condition. The size of the circles is correlated to the magnitude difference in metabolite abundance relative to the control condition. Values represent the fold-change of group averages between GDH1 or GDH2 expressing GPCs and vector control cells. Dark red colored circles indicates a p-value of <0.05 using a Welch's t-test to evaluate differences in group averages. A pink-color circle indicates a p-value between 0.05 – 0.10. (B–F) Metabolite abundance as assessed by LC/MS using the Metabolon Discovery HD4 platform. N=4 samples were cultured, collected, and

processed for each condition and metabolite abundance is graphically depicted as scaled intensity (relative abundance). One way analysis of variance and Tukey's post-hoc test was used to evaluate differences between groups, and multiplicity adjusted p-values are reported as *$p<0.05$, **$p<0.01$, ***$p<0.001$. Metabolomics data are available in Supplemental Dataset B as fold changes of group averages. (G) Gamma-glutamyl amino acids may play roles in amino acid transport and glutathione recycling.

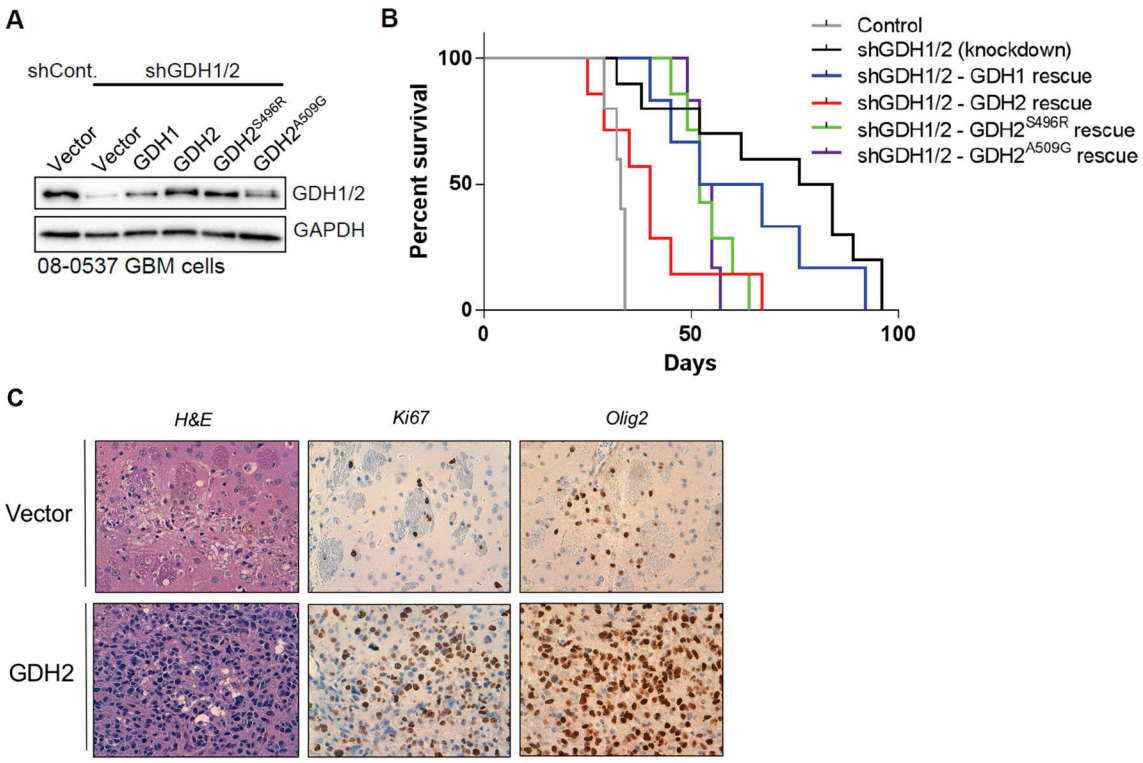

Figure 7. GDH2 promotes IDH1$^{R132H/WT}$ glioma growth in vivo

(A) GDH1/2 expression was controlled in 08-0537 cells by shRNA-mediated GDH1/2 knockdown and rescue with shRNA-resistant GDH1, GDH2, or GDH2 mutant cDNAs. (B) The survival of mice after transplantation with cell lines depicted in (A). Conditions and number of animals were shControl (n=5), shGDH1/2 (n=10), shGDH1/2-GDH1 Rescue (n=6), shGDH1/2-GDH2 Rescue (n=7), shGDH1/2-GDH2^{S496R} Rescue (n=7), shGDH1/2-GDH2^{A509G} Rescue (n=6). Data were analyzed using a log-rank test relative to the control condition. (C) Immunohistochemistry of PDGFB-IDH1$^{R132H/WT}$-TP53$^{-/-}$ murine tumors. NSCs were intracranially transplanted into n=5 mice per group and animals were euthanized at day 30 post-transplantation. Analysis of the caudate nucleus region into which cells were transplanted revealed that GDH2 expression resulted in increased Olig2 and Ki67+ cell staining.